

A catalogue of 74 new open clusters found in *Gaia* Data-Release 2

Zhi-Hong He^{1,2}, Ye Xu¹, Chao-Jie Hao^{1,2}, Zhen-Yu Wu^{3,4}, Jing-Jing Li¹

¹ Purple Mountain Observatory, CAS, No.10 Yuanhua Road, Qixia District, Nanjing 210023, China.

² University of Science and Technology of China, No.96, Jinzhai Road Baohe District, Hefei, Anhui, 230026, China

³ National Astronomical Observatories, CAS, 20A Datun Road, ChaoYang District, Beijing 100101, China

⁴ Key Laboratory of Optical Astronomy, National Astronomical Observatories, CAS, Beijing 100101, China

Abstract Based on astrometric data from *Gaia* Data-Release 2 (DR2), we employ an unsupervised machine learning method to blindly search for open star clusters in the Milky Way within the Galactic latitude range of $|b| < 20^\circ$. In addition to 2,080 known clusters, 74 new open cluster candidates are found. In this work, we present the positions, apparent radii, parallaxes, proper motions and member stars of these candidates *. Meanwhile, to obtain the physical parameters of each candidate cluster, stellar isochrones are fit to the photometric data. The results show that the apparent radii and the observed proper motion dispersions of these new candidates are consistent with those of open clusters previously identified in *Gaia* DR2.

Key words: Galaxy: open clusters and associations—methods: data analysis—surveys

1 INTRODUCTION

An open cluster (hereafter OC) is a gravitationally bound stellar system composed of dozens to thousands of stars, which presents a loose structure and is irregularly shaped (Zu & Zhao 2003). The member stars of an OC originated from the collapse of the same dense molecular environment (McKee & Ostriker 2007), and thus they have similar ages, kinematics and chemical compositions. The age of OCs can range from millions to billions of years (Dias et al. 2002; Kharchenko et al. 2013; Cantat-Gaudin et al. 2020), making them ideal places to study the evolution of stars, and they are important tracers to study the structure and kinematics of the Milky Way (e.g. Friel 1995; Lada & Lada 2003; Carraro et al. 2007; Cantat-Gaudin et al. 2020; Pang et al. 2020).

It is estimated that the total number of OCs in the Galactic disk is of the order 10^5 (Piskunov et al. 2006). The traditional method of identifying OCs is to use the positions and proper motions of groups of stars

(e.g. Sanders 1971; Slovak 1977; Zhao & He 1990; Uribe & Brieva 1994; Sánchez et al. 2010). In addition, photometric data can be used to make a colour-magnitude diagram (CMD) of a cluster to which stellar isochrones can be fit to obtain the physical parameters of the OC, such as its age, extinction and distance modulus. Before the *Gaia* era, more than 3,000 OCs had been identified and catalogued using ground-based telescopes (e.g. Dias et al. 2002; Kharchenko et al. 2013).

Gaia DR2 contains accurate parallaxes and proper motions for more than one billion stars (Gaia Collaboration et al. 2018; Lindegren et al. 2018), where stars at different distances are distinguished via stellar parallaxes. Based on *Gaia* data, searches for OCs have yielded great results. At present, $\sim 1,500$ known star clusters have been identified in *Gaia* DR2 (e.g. Cantat-Gaudin et al. 2018; Liu & Pang 2019); in addition, $\sim 1,100$ most probable new OC candidates have been recently published (e.g. Cantat-Gaudin et al. 2018, 2019; Sim et al. 2019; Liu & Pang 2019; Castro-Ginard et al. 2018, 2019, 2020; Ferreira et al. 2019, 2020; Hao et al. 2020; Qin et al. 2020).

The continuous discovery of new OCs shows that not all existing star clusters have yet been found. In this paper, relying on the precise astrometric data of *Gaia* DR2, we employ an unsupervised machine learning method to carry out blind searches for clusters within $|b| < 20^\circ$. After removing 2,080 previously reported clusters, we find 74 new OC candidates and obtain their physical parameters.

The remainder of this paper is organised as follows. In Section 2 we introduced the data. Section 3 presents our methods, including data preprocessing, the clustering algorithm and the isochrone fitting. Section 4 presents the results and provides discussions, and the conclusions are summarised in Section 5.

2 DATA

The *Gaia* satellite was launched by the European Space Agency in 2013, and its first data release was in 2016 (Gaia Collaboration et al. 2016). DR2 (Gaia Collaboration et al. 2018) provided high-precision positions and *G*-band photometric data of approximately 1.7 billion sources, of which 1.4 billion sources have both G_{BP} and G_{RP} magnitudes, and 1.3 billion stars have measured parallaxes and proper motions.

Previous studies reported that most known OCs are located near the Galactic plane $|b| < 20^\circ$ (e.g. Dias et al. 2002; Kharchenko et al. 2013). Hence, we applied three selection cuts to the *Gaia* DR2 catalogue:

- $|b| < 20^\circ$,
- $\varpi > 0.2$ mas, $\text{parallax_over_error} > 1$,
- $G < 18$ mag.

Thus, stars with $G < 18$ mag and which possess a parallax uncertainty of ~ 0.2 mas or better were added to our sample, as previously used by Cantat-Gaudin et al. (2018, 2020); Liu & Pang (2019); Ferreira et al. (2020). The final sample contained 169,137,482 stars with astrometric parameters $(l, b, \varpi, \mu_{\alpha^*}, \mu_{\delta})$, where 166,136,789 had photometric data (G, G_{BP}, G_{RP}).

3 METHOD

We used the stellar astrometric and photometric data derived in Section 2 to search for and identify new star

- Preprocess the astrometric data $(l, b, \varpi, \mu_{\alpha^*}, \mu_{\delta})$;
- Fit k_{th} NND (see Section 3.2.2) to obtain the clustering parameters, and use the clustering algorithm to obtain cluster groups; and
- Fit stellar isochrones to the photometric data $(G, G_{BP}-G_{RP})$ of the cluster candidates.

3.1 Astrometric data preparing

Following the same approach as [Hao et al. \(2020\)](#), the regions containing the data (as identified in Section 2) were divided into rectangles of size $2^\circ \times 2^\circ (|b| \leq 5^\circ)$ and $3^\circ \times 3^\circ (|b| > 5^\circ)$. Considering that the positions (l, b) and proper motions $(\mu_{\alpha^*}, \mu_{\delta})$ are relative parameters, i.e. the absolute values of distances and proper motions of stars with different parallaxes are variational, we used the projected positions, parallaxes and decomposed proper motions as input data for the clustering analysis as:

$$(d_l, d_b, \varpi, v_{\alpha^*}, v_{\delta}) = (d \cdot \sin \theta_l, d \cdot \sin \theta_b, \varpi, d \cdot \mu_{\alpha^*}, d \cdot \mu_{\delta}), \quad (1)$$

where the distance d is taken to be the inverse of the parallax, while θ_l ($\theta_l = \theta_l \cdot \cos b$) and θ_b are the angular sizes of the star and the centre of the rectangle in l and b , respectively. In addition, we calculated the median dispersion of $(d_l, d_b, \varpi, v_{\alpha^*}, v_{\delta})$ for the 2,017 OCs catalogued by [Cantat-Gaudin et al. \(2020\)](#) to standardize the above input data, so that the values in each dimension were multiples of the median dispersion of the corresponding parameter, and thus the weights of the input parameters in the process were equalized. Next, we used the DBSCAN algorithm to find clustered groups of stars.

3.2 Clustering algorithm

3.2.1 DBSCAN

The unsupervised machine learning method DBSCAN used in this work was derived from `scikit-learn` ([Pedregosa et al. 2011](#)). This algorithm was used to distinguish high-density groups from low-density regions in n -dimensional samples ([Ester et al. 1996](#)), including extracting the core members and border members located in different groups, and rejecting any outliers not located in any group. There are two parameters in the algorithm: the minimum number of data points *min_samples* and the radius ϵ , of which the latter was measured by a distance function as follows:

$$D_{ij} = \sqrt{(x_{i1} - x_{j1})^2 + (x_{i2} - x_{j2})^2 + \dots + (x_{i5} - x_{j5})^2} \quad (2)$$

where D_{ij} is the distance between data points x_i and x_j .

A core is defined as a sub-sample of the data set where *min_samples* neighbours exist within a distance equal to ϵ ; that is, the core members are located in a dense area of vector space. Border members themselves do not form cores, but they may be located close to core members (i.e. $D_{ij} < \epsilon$). In addition, outliers cannot constitute a core sample, nor can a candidate be composed of just border members, and they must be located at least ϵ from any core member. A larger *min_samples* or a smaller ϵ means a higher density required to

3.2.2 Clustering parameters: $\min_samples$ and ϵ

The parameter $\min_samples$ mainly controls the tolerance to outliers in this algorithm. Schubert et al. (2017) found that $\min_samples$ has a weak effect on the clustering results. Sander et al. (1998) suggested that $\min_samples$ can be determined as twice the value of the dimension of the data set; that is, $\min_samples = 2 \cdot \dim$, where $\dim = 5$ in this work. We tried different values of $\min_samples$ around 10, and found that the detection efficiency was highest when using $\min_samples = 8$, that is, we could obtain more cores without obvious outliers. At the same time, this value was also within the range of the best values of $\min_samples$ used by Castro-Ginard et al. (2018); Hao et al. (2020). We present the results of $\min_samples = 8$ in this article.

The parameter ϵ controls the radius of the local area of the points in the data set, and cannot be set to the default value (Schubert et al. 2017; Castro-Ginard et al. 2018). When this parameter is too small, most of the data will not be clustered; when it is too large, any adjacent clusters or outliers will merge into one group. In previous studies, Ester et al. (1996); Sander et al. (1998) selected ϵ based on the k_{th} nearest neighbour distance ($k_{th}NND$). On this basis, Schubert et al. (2017) obtained the corresponding ϵ value by observing the significant change of sorted $k_{th}NND$ plot. In the algorithm of $k_{th}NND$, the reference point is not specified as a neighbor, while that is included in the DBSCAN for density estimation, so the k value used in this work is $k = \min_samples - 1$.

In this work, the main steps to get ϵ are:

- Compute the $7_{th}NND$ histogram via *ssklearn*¹.
- Fit the $7_{th}NND$ using a bimodal Gaussian function. For gravitationally bound systems such as OCs, the intervals between the member stars in position and proper motion vectors are closer than those of field stars, so their $7_{th}NND$ s are significantly smaller than those of field stars (Castro-Ginard et al. 2018). In the $7_{th}NND$ histogram, the $7_{th}NND$ of the cluster is distributed on the leftmost end (i.e. the minimum end, Fig. 1) of the whole data set. Inspired by Castro-Ginard et al. (2018), in this work, we used a fitted $7_{th}NND$ histogram to determine ϵ as:

$$\mathbf{n} = a_1 \cdot e^{-\frac{(\mathbf{d}_{k,nn} - \mu_1)^2}{2\sigma_1^2}} + a_2 \cdot e^{-\frac{(\mathbf{d}_{k,nn} - \mu_2)^2}{2\sigma_2^2}} \quad (3)$$

where \mathbf{n} is the statistical number of $7_{th}NND$, $\mathbf{d}_{k,nn}$ is the distance, the fitted range of $\mathbf{d}_{k,nn}$ is $(0, \mathbf{d}_{k,nn} [n=\max(\mathbf{n})])$, and $(a, \mu, \sigma)_i$ are coefficients of the Gaussian functions. As shown in Fig. 1, we used two functions (curves 1 and 2) obtained by Eq. 3 to fit the $7_{th}NND$ histogram. For a data set that contains any contributions from OCs, we found that the two Gaussian functions have a real number solution (e.g. the vertical red line in Fig. 1), and it is set to be the ϵ value used in DBSCAN.

3.3 Isochrone fitting

To estimate the physical parameters of the cluster candidates, we fit isochrones to the CMDs derived from the member stars of the clusters. The isochrones used here contain logarithmic ages from 5.92 to 10.12 with

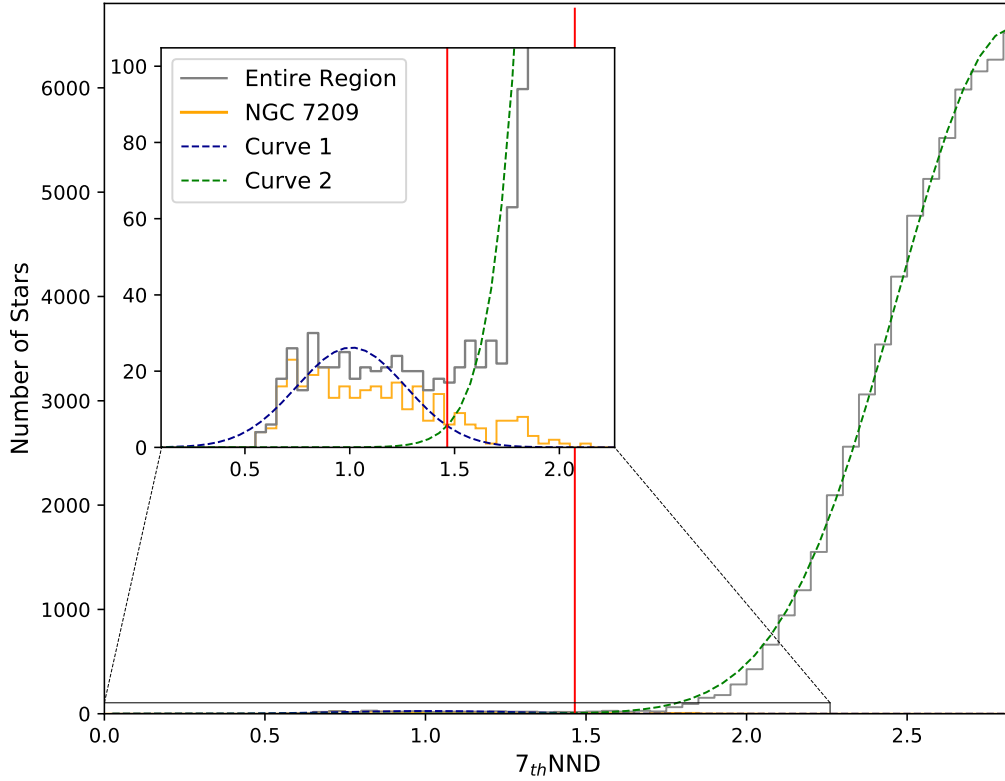


Fig. 1: Example histogram of the 7_{th} NND. The grey steps show the cumulative distribution of the star counts of 7_{th} NND in the region around cluster NGC 7209. The orange steps shows the 7_{th} NND histogram of member stars in NGC 7209, while the blue and green dashed lines show the Gaussian curves derived from Eq. 3. The red line corresponds to the chosen value of ϵ in this region, and the subplot shows a more visible zoomed-in region containing the bottom left end of the histogram.

a step of 0.02, and metal fractions from 0.015 to 0.029 with a step of 0.001¹, which come from the PARSEC library (Bressan et al. 2012) and have been updated for the *Gaia* DR2 passbands using the photometric calibrations of Evans et al. (2018). The isochrones were corrected for extinction and reddening, using an extinction curve with $R_V = 3.1$ (Cardelli et al. 1989; O’Donnell 1994).

We selected clusters whose CMDs appeared to best-fit the theoretical isochrones. Following the method of Liu & Pang (2019), the mean square distances to the isochrones were used to match the observed cluster members using Eq. 4:

$$\bar{d}^2 = \frac{\sum_{k=1}^n (\mathbf{x}_k - \mathbf{x}_{k,nn})^2}{n} \quad (4)$$

where n is the number of core members (Section 3.2.1) in a cluster, and \mathbf{x} , $\mathbf{x}_{k,nn}$ are the positions of the member stars and the points on the isochrone that are closest to the member stars, respectively. At the same time, we also obtained the standard deviation of the square distance, σ_{d^2} , which was used to reflect the dispersion of the core members along the isochrones (Section 4.2).

4 RESULTS AND DISCUSSION

We applied the algorithm described in Section 3.2.1 to about 170 million stars. Since some clusters were located near the edges of each rectangle (Section 3.1), in order not to find duplicate clusters or substructures of known clusters, we merged the cluster results within a range of 3σ of the astrometric data ($l, b, \varpi, \mu_{\alpha^*}, \mu_{\delta}$); meanwhile, a visual inspection was also adopted. Moreover, to reduce the influence of outliers, we omitted clustering results with $n_{core} < 5$. After that, we obtained 3,066 groups with a total of 371,362 members, of which 261,377 were core members. Thereafter, we removed all known OCs from this sample (Section 4.1).

4.1 Cross matching with previous catalogues

4.1.1 OCs in Gaia DR2

Our first cross-matched catalogue contained OCs derived from *Gaia* DR2. In the previous studies, Sim et al. (2019) found 207 new OCs within 1 kpc of solar system, while Liu & Pang (2019) found 2,443 star clusters and candidates, 76 of which were most probable new star clusters. Cantat-Gaudin et al. (2020) re-visited 2017 OCs, including the catalogues of Cantat-Gaudin et al. (2018, 2019); Cantat-Gaudin & Anders (2020); Castro-Ginard et al. (2018, 2019, 2020), and a portion of OCs published by Sim et al. (2019); Liu & Pang (2019). In addition, we considered the 28, 16 and four new OCs recently been found by Ferreira et al. (2019, 2020); Hao et al. (2020); Qin et al. (2020), respectively.

Most OCs are observed to have projected spatial extents up to nearly 15 pc (Gaia Collaboration et al. 2017) from the cluster centres, such as the apparent radii of OCs found in *Gaia* DR2 by Cantat-Gaudin & Anders (2020). Therefore, within the range of the maximum distance from the centre of an OC considered here (15 pc, 5σ dispersion) within (l, b) , we extracted the reported clusters adjacent to the center of each identified group. Then, in the range of a 5σ dispersion about $(\varpi, \mu_{\alpha^*}, \mu_{\delta})$, the extracted clusters were matched, and the matched ones were removed. Finally, a total of 1,978 reported star clusters were removed.

4.1.2 OCs before Gaia

We continue to match the remaining groups with the catalogues published by Dias et al. (2002, D02) and Kharchenko et al. (2013, K13). To do this we made use of the root mean square (RMS) differences of the ages and distance moduli between the K13 clusters and cross-matched clusters identified in *Gaia* DR2 by Cantat-Gaudin et al. (2020), which reflected the differences of these parameters between the re-identified clusters in *Gaia* DR2 and the previous known OCs. We selected clusters in a range of $\max(15 \text{ pc}, 5\sigma \text{ dispersion})$ about (l, b) , and then compared the ages and distance moduli of the remaining groups with those of the K13 and D02 clusters within a 2-RMS level. In all, 46 groups were removed.

Next, Bica et al. (2019, B19) constructed a sample 4,384 open/globular clusters, cluster candidates and cluster remnants, where most of them were previously catalogued by D02 and K13. We also matched the objects found by B19 with the remaining groups, where the radius of each matched cluster had to satisfy $d_r \leq \text{radius} \leq r_{15pc}$, where d_r is the angular size between the matched group and the reported cluster. Although most star clusters could be physically distinguished, we also performed visual checks of the

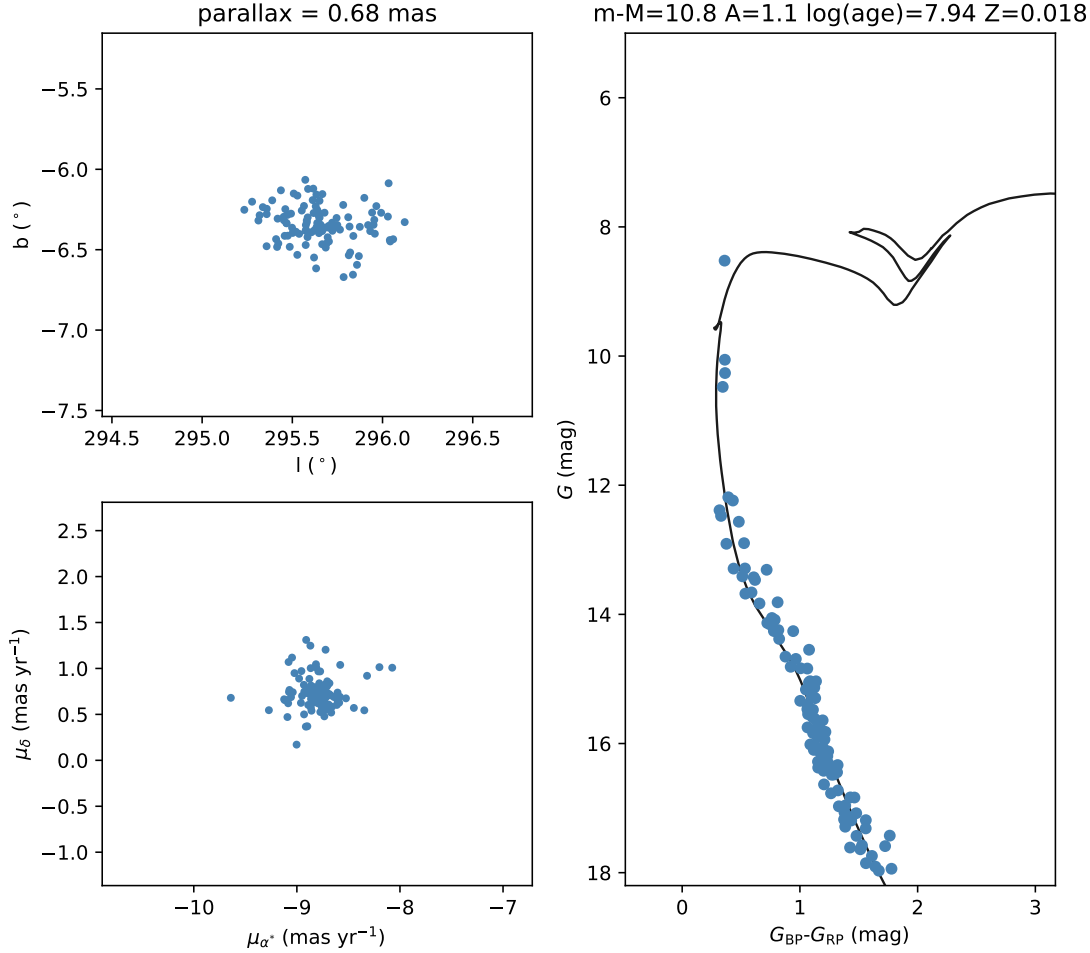


Fig. 2: Example position and proper motion distributions, and CMDs of the member stars in a cluster candidate (NO.016 in Table 1). The black line presents the best-fitting isochrone.

positions catalogued by B19, and we included two of them in the final table (Table 1). After all the checking and filtering, 986 groups remained in our collated sample.

4.2 New cluster candidates

To find any probable new star clusters among the 986 groups, we selected clusters whose CMDs coincided well with the stellar isochrones (Section 3.3). Inspired by Liu & Pang (2019), we first adopted criteria of $n > 30$; $\bar{d}^2 < 0.02$; $\sigma_{d^2} < 0.04$. After application of these criteria, 168 clusters with well-fitting isochrones remained in the sample. Furthermore, we performed visual inspections under careful consideration of the distributions of the positions and proper motions, and the CMDs of the remaining clusters. After that, 74 OC candidates remained. In Table 1, we have presented the locations and sizes of these candidates, including their parallaxes, proper motions and corresponding 1σ dispersions, which have also been presented in the works of Cantat-Gaudin & Anders (2020); Cantat-Gaudin et al. (2020) in the same way. The distance moduli, ages, extinction and metal fraction values of these candidates are also provided. The distributions, proper motions, CMDs (e.g. Fig. 2) and member stars of each cluster are also shown in electric form.

Table 1: Parameters of the newly identified OC candidates.

NO.	l ($^{\circ}$)	b ($^{\circ}$)	θ (deg)	$n(n_{core})$	$\varpi(\sigma_{\varpi})$ (mas)	$\mu_{\alpha^*}(\sigma_{\mu_{\alpha^*}})$ (mas yr $^{-1}$)	$\mu_{\delta}(\sigma_{\mu_{\delta}})$ (mas yr $^{-1}$)	$m - M$ (mag)	log(age/yr)	A_G (mag)	Z
001	94.203	-5.840	0.20	45(20)	0.67(0.03)	1.28(0.16)	-2.34(0.12)	10.9	8.40	1.0	0.016
002	215.533	4.061	0.11	44(22)	0.50(0.05)	-0.51(0.11)	-1.48(0.11)	11.5	8.12	0.9	0.025
003	237.912 ^a	0.449	0.18	143(75)	0.55(0.05)	-1.38(0.13)	1.24(0.13)	11.4	8.36	0.6	0.026
004	116.192	-1.297	0.09	32(15)	0.37(0.03)	-1.78(0.09)	-1.02(0.06)	12.0	7.82	2.2	0.021
005	228.825	1.196	0.26	32(15)	1.18(0.03)	-1.41(0.18)	0.44(0.26)	9.7	8.04	0.4	0.028
006	354.888	-1.335	0.14	70(45)	1.05(0.05)	1.12(0.12)	-0.09(0.11)	9.3	8.84	0.3	0.025
007	11.026	-1.960	0.13	52(25)	0.79(0.05)	-0.06(0.13)	-1.62(0.12)	10.5	7.48	0.9	0.024
008	87.492 ^a	-3.675	0.37	50(24)	0.85(0.04)	0.05(0.14)	-4.35(0.13)	10.4	8.54	1.0	0.027
009	241.773	0.143	0.17	41(13)	0.38(0.03)	-1.63(0.09)	1.31(0.12)	11.9	7.98	0.6	0.026
010	339.546	-4.429	0.22	67(45)	1.09(0.05)	-1.33(0.14)	-2.67(0.15)	9.9	7.98	1.0	0.027
011	261.833	-9.192	0.43	101(39)	0.63(0.04)	-3.79(0.18)	4.92(0.18)	11.3	7.44	0.9	0.024
012	202.447	-5.870	0.23	54(28)	0.86(0.06)	-0.01(0.18)	-1.43(0.17)	10.4	7.58	0.9	0.021
013	315.674	1.631	0.25	57(36)	0.87(0.04)	-1.20(0.10)	-3.11(0.13)	10.3	7.54	1.1	0.017
014	314.563	2.660	0.15	46(16)	0.52(0.02)	-2.66(0.12)	-2.72(0.10)	11.3	8.52	0.8	0.027
015	259.105	-2.451	0.24	81(41)	0.70(0.04)	-5.76(0.14)	4.21(0.14)	10.9	8.02	1.1	0.027
016	295.638	-6.345	0.21	107(63)	0.68(0.04)	-8.80(0.13)	0.72(0.14)	10.8	7.94	1.1	0.018
017	226.571	0.150	0.24	43(21)	0.93(0.07)	-2.11(0.19)	-0.18(0.13)	10.3	8.42	0.7	0.024
018	165.573	-2.123	0.30	46(19)	0.95(0.07)	-0.40(0.17)	-3.05(0.14)	9.9	7.54	0.9	0.019
019	210.343	-4.082	0.14	41(24)	0.76(0.05)	1.44(0.10)	-1.31(0.10)	10.6	8.60	1.5	0.017
020	303.139	-0.852	0.09	59(28)	0.63(0.07)	-6.34(0.19)	-1.58(0.14)	10.6	7.94	1.7	0.024
021	224.698	3.430	0.11	46(19)	0.46(0.06)	-0.80(0.12)	-0.87(0.11)	11.1	9.02	0.1	0.019
022	224.178	1.248	0.22	47(30)	0.86(0.06)	-0.57(0.11)	0.83(0.20)	10.5	7.76	0.7	0.016
023	102.341	-2.235	0.10	38(26)	0.68(0.04)	1.71(0.09)	-2.25(0.13)	11.0	8.72	1.1	0.028
024	236.831	2.172	0.10	39(27)	0.59(0.05)	-0.99(0.07)	0.59(0.10)	11.2	7.96	1.0	0.025
025	312.078	-2.372	0.06	34(14)	0.48(0.03)	-4.72(0.08)	-3.13(0.15)	11.2	7.60	1.2	0.021
026	240.457	-4.731	0.31	85(55)	0.80(0.05)	-4.29(0.13)	3.85(0.11)	10.5	7.44	0.1	0.026
027	333.864	-4.275	0.13	32(13)	0.59(0.01)	-1.58(0.14)	-4.01(0.07)	11.1	8.66	1.1	0.028
028	100.808	0.620	0.14	88(42)	0.64(0.05)	-2.01(0.16)	-1.63(0.12)	10.8	7.92	2.2	0.027
029	2.373	-0.261	0.22	63(45)	1.66(0.05)	0.89(0.19)	-5.12(0.18)	9.0	7.70	0.8	0.023
030	24.838	-6.092	0.22	43(27)	0.94(0.04)	1.13(0.11)	0.84(0.10)	10.3	8.50	1.1	0.026
031	86.396	-0.476	0.04	33(16)	0.49(0.03)	-2.51(0.13)	-4.52(0.14)	11.0	8.14	1.7	0.020
032	221.101	-1.049	0.19	51(30)	0.88(0.04)	-1.59(0.13)	-3.46(0.14)	10.5	8.54	0.8	0.025
033	343.054	2.668	0.18	100(56)	0.90(0.05)	1.42(0.19)	-2.98(0.16)	10.1	7.64	1.2	0.016
034	309.876	1.271	0.14	41(27)	0.75(0.04)	-7.20(0.09)	-2.26(0.11)	10.4	7.98	0.8	0.025
035	161.079	-0.654	0.09	34(17)	0.52(0.05)	1.43(0.13)	-2.11(0.26)	11.5	8.44	1.0	0.024

036	263.281	-6.758	0.27	32(15)	0.93(0.04)	-5.61(0.15)	5.11(0.15)	10.1	7.88	0.4	0.027
037	20.457	-0.866	0.15	37(19)	0.92(0.05)	-0.06(0.14)	-3.05(0.12)	9.9	8.82	1.4	0.023
038	178.173	2.255	0.15	30(14)	0.71(0.05)	0.49(0.15)	-3.81(0.10)	10.8	8.46	0.7	0.026
039	121.599	6.001	0.33	37(21)	0.96(0.03)	-1.53(0.14)	-0.57(0.11)	9.5	7.94	1.9	0.016
040	70.424	-1.231	0.03	50(38)	0.48(0.03)	-3.83(0.09)	-5.30(0.14)	11.1	8.24	3.9	0.024
041	92.224	-6.323	0.61	68(29)	0.78(0.04)	2.15(0.24)	-0.02(0.11)	10.2	8.88	0.4	0.017
042	252.836	-1.370	0.31	66(36)	0.86(0.04)	-4.78(0.10)	2.97(0.15)	10.4	7.96	0.7	0.026
043	237.960	0.637	0.19	90(41)	0.66(0.04)	-2.52(0.18)	1.65(0.12)	10.9	8.46	0.3	0.026
044	134.977	1.725	0.18	34(20)	0.67(0.03)	-0.91(0.18)	-0.46(0.13)	10.8	7.66	1.8	0.017
045	111.351	-2.453	0.14	59(40)	0.99(0.04)	-0.42(0.12)	-0.83(0.12)	9.9	7.90	2.2	0.020
046	68.596	2.636	0.09	56(37)	0.49(0.04)	-2.51(0.10)	-3.43(0.11)	11.3	8.34	1.7	0.018
047	327.232	-1.331	0.07	33(11)	0.57(0.03)	-3.95(0.16)	-5.16(0.11)	10.6	8.78	2.0	0.024
048	225.173	5.548	0.15	33(17)	0.90(0.08)	-3.59(0.14)	0.99(0.11)	10.2	7.98	0.1	0.026
049	169.769	-1.966	0.13	33(17)	0.60(0.04)	1.15(0.13)	-3.97(0.09)	10.9	8.18	1.2	0.024
050	203.158	-2.565	0.07	41(20)	0.49(0.05)	-0.90(0.16)	-0.24(0.10)	11.7	8.16	1.0	0.019
051	19.445	-2.247	0.08	45(23)	0.56(0.04)	0.67(0.11)	-0.14(0.11)	10.9	8.10	1.9	0.025
052	220.279	0.592	0.17	35(20)	0.60(0.04)	-0.26(0.11)	-0.64(0.16)	10.7	7.92	0.5	0.021
053	174.786	-1.207	0.14	35(13)	0.64(0.06)	1.41(0.17)	-3.54(0.18)	11.2	7.54	1.1	0.023
054	221.571	0.052	0.16	50(33)	0.93(0.02)	-3.94(0.15)	1.14(0.14)	10.3	8.42	0.4	0.028
055	298.570	-8.573	0.35	42(18)	0.73(0.05)	-4.05(0.16)	-0.69(0.13)	10.5	7.78	0.9	0.017
056	92.545	-3.423	0.10	34(18)	0.78(0.05)	1.44(0.08)	-0.35(0.11)	10.6	7.90	0.9	0.027
057	16.639	-1.919	0.13	40(19)	0.86(0.05)	-2.70(0.08)	-3.56(0.08)	10.1	8.48	0.7	0.028
058	203.355	0.556	0.12	38(15)	0.48(0.04)	0.03(0.11)	-1.38(0.07)	11.3	7.28	1.1	0.018
059	235.209	1.629	0.06	35(20)	0.41(0.04)	-2.23(0.10)	2.19(0.09)	12.0	7.52	1.5	0.021
060	210.929	5.473	0.13	55(29)	0.48(0.04)	-0.39(0.11)	-1.66(0.12)	11.5	8.30	0.9	0.022
061	221.759	-4.652	0.14	73(37)	0.50(0.04)	-1.28(0.12)	1.25(0.15)	11.6	8.28	1.4	0.020
062	233.570	-4.761	0.10	36(14)	0.49(0.05)	-1.60(0.14)	0.67(0.13)	11.3	8.38	1.6	0.024
063	133.389	-0.837	0.08	39(21)	0.63(0.06)	-0.89(0.09)	0.16(0.18)	10.8	8.00	2.1	0.022
064	293.050	-6.779	0.28	46(27)	0.93(0.04)	-7.41(0.14)	1.72(0.19)	10.2	7.90	1.0	0.022
065	245.796	3.234	0.19	32(23)	0.99(0.04)	-3.93(0.11)	2.00(0.10)	10.1	8.20	0.2	0.028
066	14.837	1.394	0.05	33(13)	0.61(0.03)	-0.25(0.12)	-1.73(0.15)	11.4	6.80	1.4	0.028
067	323.479	-2.512	0.06	33(16)	0.54(0.03)	-2.17(0.07)	-3.52(0.11)	10.7	8.38	1.8	0.028
068	262.909	-4.363	0.38	71(31)	0.82(0.05)	-6.29(0.20)	5.02(0.33)	10.3	7.78	0.7	0.017
069	234.158	-12.181	0.33	93(66)	0.94(0.06)	-1.52(0.12)	2.45(0.15)	10.1	8.60	0.4	0.018
070	254.535	-6.050	0.28	31(11)	0.82(0.05)	-4.06(0.16)	4.59(0.21)	10.3	7.98	0.6	0.027
071	255.762	-4.530	0.14	36(18)	0.67(0.04)	-4.20(0.14)	3.38(0.08)	11.1	8.52	1.2	0.028
072	217.519	0.474	0.22	35(12)	0.64(0.04)	-0.15(0.09)	-0.80(0.10)	11.3	7.86	0.5	0.028
073	147.486	4.112	0.15	68(36)	0.69(0.06)	1.04(0.10)	-1.06(0.15)	10.4	7.82	2.1	0.018
074	216.760	-0.834	0.05	35(20)	0.42(0.05)	-1.81(0.11)	1.07(0.07)	11.6	8.76	1.2	0.019

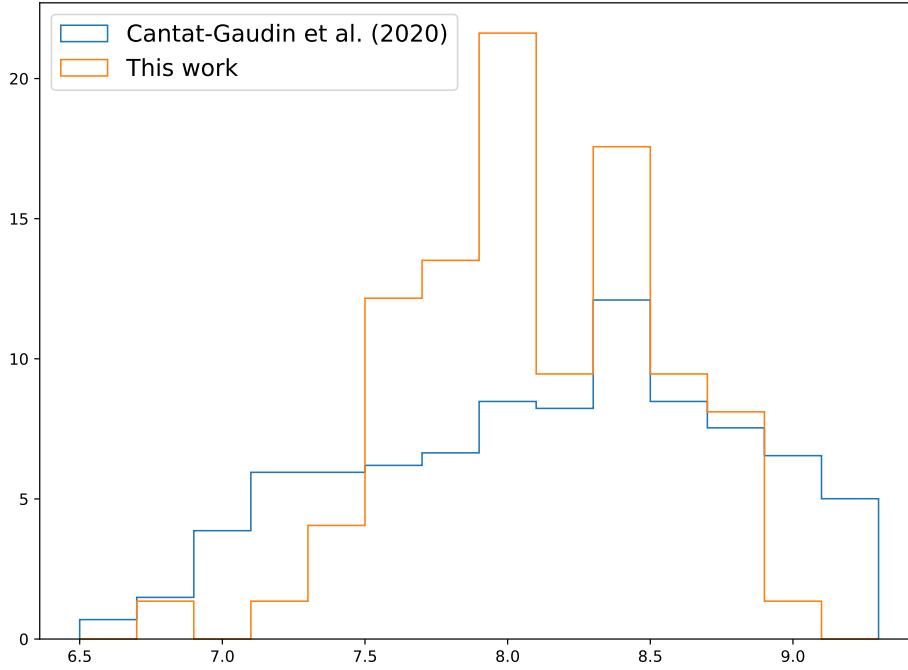


Fig. 3: Frequency distribution of the logarithmic ages of the cluster candidates derived in this study, which have been compared to those of *Gaia* DR2 confirmed OCs (Cantat-Gaudin et al. 2020).

^a Adjacent to the cluster catalogued by Bica et al. (2019).

As shown in Fig. 3, the isochrones show that the ages of most of the new OC candidates are in the range of $\log(\text{age/yr}) = (7.5, 8.5)$, and two extreme values are located at $\log(\text{age/yr}) = 8.0$ and 8.4 . These results are similar to the age distributions of the OCs presented by Cantat-Gaudin et al. (2020, CG20). However, the peak value of $\log(\text{age/yr}) = 8.0$ may be due to bias caused by the new cluster candidates found in this work forming an incomplete sample. In addition, as shown in Fig. 4, the apparent radii of the new star cluster candidates are below 15 pc, which is consistent with the distributions of apparent radii of OCs catalogued by CG20.

As a gravitationally bound system, member stars of an OC have much smaller internal velocity dispersions than field stars. Radial velocities derived from high-resolution spectroscopic observations have shown that the internal velocity dispersion of OCs are generally less than 2 km s^{-1} (e.g. Donati et al. 2014; Cantat-Gaudin et al. 2014; Vereshchagin & Chupina 2016; Overbeek et al. 2017). Meanwhile, the observed proper motion dispersions of the clusters found in *Gaia* DR2 are correlated with their parallaxes (Cantat-Gaudin & Anders 2020; Ferreira et al. 2020). As shown in Fig. 5, the proper motion dispersions of the new star cluster candidates found in this work are below 0.5 mas yr^{-1} , and the resolved velocity dispersions of most candidates are below 1 km s^{-1} , which are consistent with the results of star clusters found in *Gaia* DR2 by

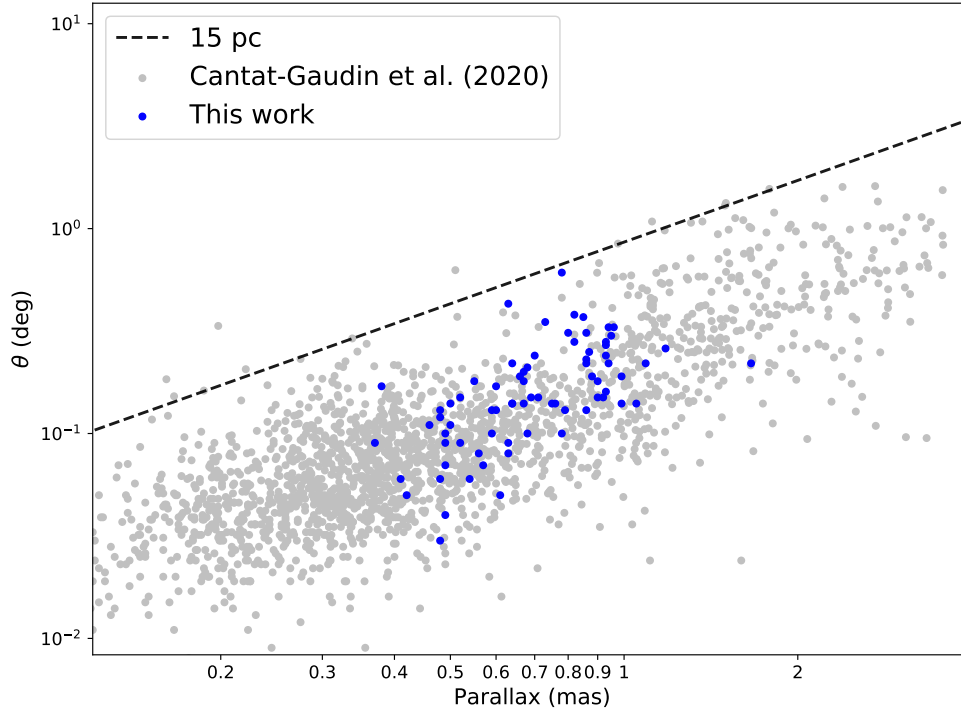


Fig. 4: Apparent radius as a function of parallax for the cluster candidates discovered in this work (blue dots). The grey dots show the OCs cataloged by Cantat-Gaudin et al. (2020) in *Gaia* DR2. The black dashed line indicates an angular size corresponding to 15 pc (Cantat-Gaudin & Anders 2020).

5 CONCLUSION

Adopting the clustering algorithm DBSCAN, we used the positions, parallaxes, and proper motions of nearly 170 million stars within the galactic latitude range $|b| < 20^\circ$ and parallax $\varpi > 0.2$ mas in *Gaia* DR2 to search for unknown OCs. We cross-matched our initial sample with previous star cluster catalogues, and after performing several vetting stages, we obtained a catalogue of 74 new OC candidates. We fitted isochrones to these candidates and obtained their corresponding physical parameters. The apparent radii and observed proper motion dispersions of the new cluster candidates were consistent with those of OCs previously found in *Gaia* DR2.

The detection of new OC candidates shows that there are still some missed OCs in the *Gaia* data. *Gaia* EDR3 will be initially released in December 2020, with the complete release due the first half of 2022, which will contain higher precision parallaxes, proper motions and photometric data. Therefore, the newly discovered OC candidates in this work can be further confirmed their natures, and more star clusters are expected to be found in future works.

6 ACKNOWLEDGEMENTS

This work has made use of data from the European Space Agency (ESA) mission *Gaia* (<https://www.ESA.int>).

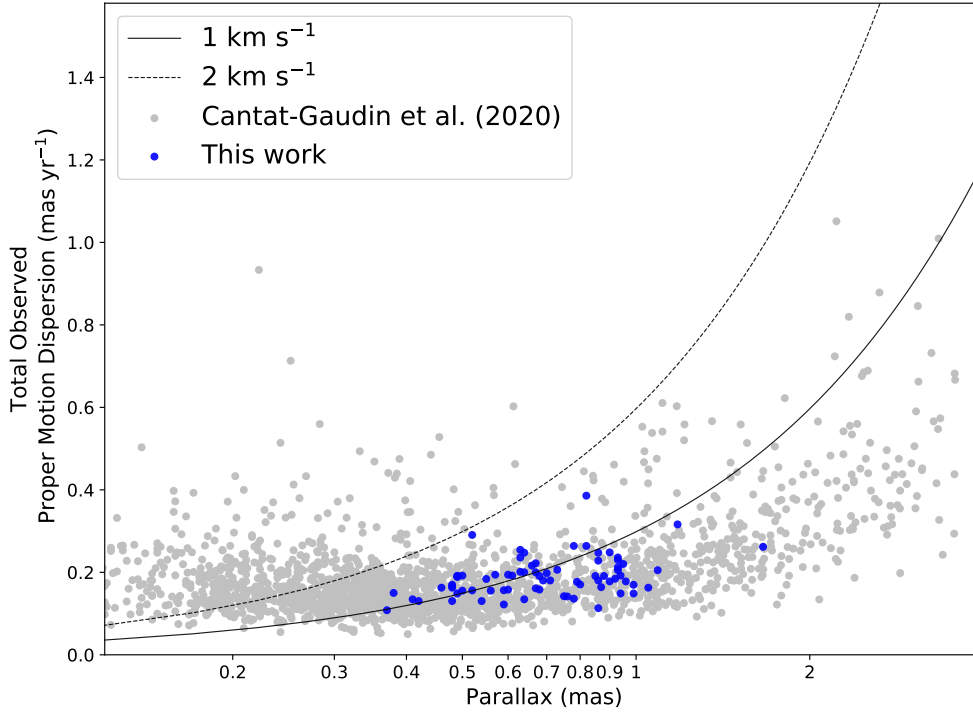


Fig. 5: Total proper motion dispersion as a function of parallax for the cluster candidates discovered in this work (blue dots). The grey dots show the OCs cataloged by Cantat-Gaudin et al. (2020) in *Gaia* DR2. The black solid and dashed lines show the proper motion dispersions corresponding to theoretical 1-D velocity dispersions of 1 and 2 km s⁻¹, respectively, in the absence of any measurement errors (Cantat-Gaudin & Anders 2020).

[//www.cosmos.esa.int/web/Gaia/dpac/consortium](http://www.cosmos.esa.int/web/Gaia/dpac/consortium)). Funding for the DPAC has been provided by national institutions, in particular the institutions participating in the *Gaia* Multilateral Agreement. This work was funded by the NSFC (grant numbers 11933011, 11873019, and 11673066), and by the Key Laboratory for Radio Astronomy. This research has made use of the open-source Python packages *Astropy* (Price-Whelan et al. 2018), *NumPy* (Oliphant 2006), *scikit-learn* (Pedregosa et al. 2011) and *Pandas* (McKinney et al. 2010). The figures in this article were created using *Matplotlib* (Hunter 2007).

References

- Bica, E., Pavani, D. B., Bonatto, C. J., & Lima, E. F. 2019, *AJ*, 157, 12
- Bressan, A., Marigo, P., Girardi, L., et al. 2012, *MNRAS*, 427, 127
- Cantat-Gaudin, T., & Anders, F. 2020, *A&A*, 633, A99
- Cantat-Gaudin, T., Vallenari, A., Zaggia, S., et al. 2014, *A&A*, 569, A17
- Cantat-Gaudin, T., Jordi, C., Vallenari, A., et al. 2018, *A&A*, 618, A93
- Cantat-Gaudin, T., Krone-Martins, A., Sedaghat, N., et al. 2019, *A&A*, 624, A126

- Cardelli, J. A., Clayton, G. C., & Mathis, J. S. 1989, *ApJ*, 345, 245
- Carraro, G., Geisler, D., Villanova, S., Frinchaboy, P. M., & Majewski, S. R. 2007, *A&A*, 476, 217
- Castro-Ginard, A., Jordi, C., Luri, X., Cantat-Gaudin, T., & Balaguer-Núñez, L. 2019, *A&A*, 627, A35
- Castro-Ginard, A., Jordi, C., Luri, X., et al. 2018, *A&A*, 618, A59
- . 2020, *A&A*, 635, A45
- Dias, W. S., Alessi, B. S., Moitinho, A., & Lépine, J. R. D. 2002, *A&A*, 389, 871
- Donati, P., Cantat Gaudin, T., Bragaglia, A., et al. 2014, *A&A*, 561, A94
- Ester, M., Kriegel, H.-P., Sander, J., & Xu, X. 1996, in *Proc. of 2nd International Conference on Knowledge Discovery and Data Mining (KDD-96)*, 226–231
- Evans, D. W., Riello, M., De Angeli, F., et al. 2018, *A&A*, 616, A4
- Ferreira, F. A., Corradi, W. J. B., Maia, F. F. S., Angelo, M. S., & Santos, J. F. C., J. 2020, *MNRAS*, 496, 2021
- Ferreira, F. A., Santos, J. F. C., Corradi, W. J. B., Maia, F. F. S., & Angelo, M. S. 2019, *MNRAS*, 483, 5508
- Friel, E. D. 1995, *ARA&A*, 33, 381
- Gaia Collaboration, Prusti, T., de Bruijne, J. H. J., et al. 2016, *A&A*, 595, A1
- Gaia Collaboration, van Leeuwen, F., Vallenari, A., et al. 2017, *A&A*, 601, A19
- Gaia Collaboration, Brown, A. G. A., Vallenari, A., et al. 2018, *A&A*, 616, A1
- Hao, C., Xu, Y., Wu, Z., He, Z., & Bian, S. 2020, *PASP*, 132, 034502
- Hunter, J. D. 2007, *Computing in science & engineering*, 9, 90
- Kharchenko, N. V., Piskunov, A. E., Schilbach, E., Röser, S., & Scholz, R. D. 2013, *A&A*, 558, A53
- Lada, C. J., & Lada, E. A. 2003, *ARA&A*, 41, 57
- Lindegren, L., Hernández, J., Bombrun, A., et al. 2018, *A&A*, 616, A2
- Liu, L., & Pang, X. 2019, *ApJS*, 245, 32
- McKee, C. F., & Ostriker, E. C. 2007, *ARA&A*, 45, 565
- McKinney, W., et al. 2010, in *Proceedings of the 9th Python in Science Conference*, Vol. 445, Austin, TX, 51–56
- O’Donnell, J. E. 1994, *ApJ*, 422, 158
- Oliphant, T. E. 2006, *A guide to NumPy*, Vol. 1 (Trelgol Publishing USA)
- Overbeek, J. C., Friel, E. D., Donati, P., et al. 2017, *A&A*, 598, A68
- Pang, X., Li, Y., Tang, S.-Y., Pasquato, M., & Kouwenhoven, M. B. N. 2020, *ApJ*, 900, L4
- Pedregosa, F., Varoquaux, G., Gramfort, A., et al. 2011, *Journal of Machine Learning Research*, 12, 2825
- Piskunov, A. E., Kharchenko, N. V., Röser, S., Schilbach, E., & Scholz, R. D. 2006, *A&A*, 445, 545
- Price-Whelan, A. M., Sipőcz, B., Günther, H., et al. 2018, *The Astronomical Journal*, 156, 123
- Qin, S.-m., Li, J., Chen, L., & Zhong, J. 2020, *arXiv e-prints*, arXiv:2008.07164
- Sánchez, N., Vicente, B., & Alfaro, E. J. 2010, *A&A*, 510, A78
- Sander, J., Ester, M., Kriegel, H.-P., & Xu, X. 1998, *Data Min. Knowl. Discov.*, 2, 169
- Sanders, W. L. 1971, *A&A*, 14, 226
- Schubert, E., Sander, J., Ester, M., Kriegel, H.-P., & Xu, X. 2017, *ACM Trans. Database Syst.*, 42, 19:1
- Sim, G., Lee, S. H., Ann, H. B., & Kim, S. 2019, *Journal of Korean Astronomical Society*, 52, 145

Slovak, M. H. 1977, *AJ*, 82, 818

Uribe, A., & Brieva, E. 1994, *Ap&SS*, 214, 171

Vereshchagin, S. V., & Chupina, N. V. 2016, *Baltic Astronomy*, 25, 432

Zhao, J. L., & He, Y. P. 1990, *A&A*, 237, 54

Zu, Z. L., & Zhao, J. L. 2003, *Progress in Astronomy*, 21, 152